ARTICLE

Supporting Information

Efficient Stable Graphene-based Perovskite Solar Cells with High Flexibility in Device Assembling via Modular Architecture Design

Chunyang Zhang,[a] Shi Wang,[a] Hong Zhang,[b] Yulin Feng,[c] Wenming Tian,[d] Ying Yan,[e] Jiming Bian,*[c] Yuchen Wang,[a] Shengye Jin,[d] Shaik Mohammed Zakeeruddin*[b], Michael Grätzel [b] and Yantao Shi *[a]

Experimental

Materials and Reagents: All the chemicals were used as received, including $SnCl_2$ $2H_2O$ (98%, Alfa Aesar), CH_3NH_3Br (MABr, Dyesol), $CH(NH_2)_2I$ (FAI, Xi'an Polymer Light Technology Corp), CsI (99.999%, Sigma Aldrich), PbI_2 (99.99%, TCI), $PbBr_2$ (＞98.0%, TCI), , spiro-OMeTAD (99.7%, Lumtec), 4-tert-butylpyridine (TBP, 96%, Sigma Aldrich), bis(trifluoromethane)sulfonimide lithium salt (Li-TFSI, 99.95%, Sigma Aldrich), isopropanol (99.5%, Sigma Aldrich), dimethyl sulfoxide (DMSO, 99.9%, Sigma Aldrich), dimethylformamide (DMF, 99.8%, Sigma Aldrich), acetonitrile (99.8%, Sigma Aldrich), chlorobenzene (99.8%, Sigma Aldrich), α, α, α-Trifluorotoluene (≥99%, Sigma Aldrich), deionized water, ethanol (Sinopharm Chemical Reagent Co., Ltd), acetone (Sinopharm Chemical Reagent Co., Ltd), carbon black (Cabot BP 2000, America), graphite flake (99%, Alfa Aesar), graphene (XFNANO). FTO (7 Ω sq^{-1}) was purchased from Yingkou OPV Tech New Energy Co., Ltd.

Fabrication of modular C-PSCs: 20 mg carbon material, i.e. carbon black, graphite or graphene, were dispersed into 5 ml isopropanol through ball-milling for 12 h to obtain a homogeneous dispersion. FTO glasses were patterned through etching with zinc power and 4 M HCl, and then rinsed with cleaning fluid, deionized water, ethanol, acetone and isopropanol sequentially. The 0.1 M SnO_2 sol was prepared according to our previous work. Typically, the 0.1 M $SnCl_2$ $2H_2O$ isopropanol solution was refluxed at 85 °C in the air for 3 h to obtain SnO_2 sol, then being spin-coated on FTO at 2000 rpm for 30 s and heated at 80 °C for 1 h in the air. Then, the as-deposited SnO_2 ETL was treated with

UV-Ozone (BZS250GF-TC, China) for 20 min. After deposition of this ETL, the perovskite was deposited through one-step spin coating method. Firstly, FAI (1 M), PbI_2 (1.1 M), MABr (0.2 M) $PbBr_2$ (0.2 M) were dissolved in 1 ml mixed solvent of DMF and DMSO (volume ratio is 4:1). The precursor solution was stirred at 60 ^oC for 2 h. Then 1 M DMSO solution of CsI was added to above perovskite solution in the 5:95 ratios. Secondly, 100 µl mixed perovskite precursor solution was spread on the ETL through two-step spin coating process (1000 rpm for 10 s and 6000 rpm for 30 s). 300 µl α, α, α-trifluorotoluene was poured on the spinning substrate 20 s prior to the end of the second step program. The substrate was placed on a hotplate kept at 85 ^oC for 40 min. The precursor solution of spiro-OMeTAD was prepared through dissolving 72.3 mg spiro-OMeTAD, 29 µl TBP, 17.5 µl Li-TFSI acetonitrile solution (520 mg/ml) in 1 ml chlorobenzene. 50 µl above spiro-OMeTAD precursor solution was spin coated on the perovskite layer at 3000 rpm for 30 s. Finally, 100 µl isopropanol dispersion of carbon material was sprayed on above Semi-cell which was fixed on 85 ^oC hotplate through using the tape to speed up solvent evaporation, and semi-cell A was obtained. Subsequently, 100 µl isopropanol dispersion of carbon material was sprayed on FTO or Al foil which was fixed on 85 ^oC hotplate through using the tape to speed up solvent evaporation, then, the charge collector B was obtained. Finally, modular C-PSC was assembled by stacking semi-cell A and charge collector B together without extra processing.

Characterizations: The sample morphologies were studied through scanning electron microscopy (SEM, SU8220, JAPAN). HRTEM analysis were carried out on a JEM-2100 microscope. Electrochemical impedance spectroscopy (EIS) was measured via an electrochemical workstation (Zennium Zahner, Germany) in dark, under 0.3 V forward bias and with 20 mV amplitude of AC perturbation ranging from 100 mHz to 2 MHz. We measure the *J-V* characteristics of the modular PSCs using a Keithley 2450 digital source meter at a scan speed of 100 mV s^{-1}. The simulated AM 1.5G sunlight with an irradiance equivalent to 100 mW cm^{-2} was generated through an Oriel Solar 3A solar simulators and the intensity was calibrated with standards Si reference cell (PECSI01). The modular C-PSCs were masked using a black metal mask with an aperture area of 0.09 cm^2 or 1.3 cm^2. The steady-state output of photocurrent and PCE were measured via a Keithley 2450 digital source meter under a certain bias. The incident photon-to-electron conversion efficiency (IPCE) spectra were recorded by a set of equipment which including a

potentiostat, a monochromator, and a xenon light source. Time-resolved fluorescence measurements were performed using a photoluminescence (PL)-scanned imaging microscope coupled with a time-correlated single photon counting (TCSPC) module. Excitation of the sample was achieved with a supercontinuum white-light laser (SC400-PP, Fianium, UK) of 450 nm wavelength, 1 MHz repetition rate and ~6 ps pulse width. The PL signal was collected using a high-speed detector (HPM-100-40, Hamamatsu, Japan) with a 710 nm long pass filter and 747 ± 16.5 nm band pass filter.

Table S1: The market price of typical carbon materials and highly purified Au/Ag for thermal evaporation.

Sample	Price (RMB/g)
Highly purified Au	822
Highly purified Ag	120
Carbon powder	Less than 1

Table S2. A summary of device structure and photovoltaic performance of C-PSCs.

Device structure	Method	Carbon Sources	Area [cm^2]	V_{oc} [V]	J_{sc} [mA cm^{-2}]	FF [%]	PCE [%]	Ref.
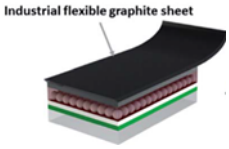	SP[a)]	Graphite paper	N/A	0.91	18.15	65	10.73	11
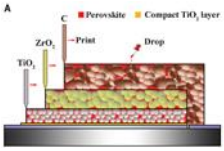	SP	CG[f)]	0.07	0.84	21.1	65	11.6	6
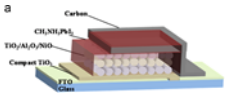	SP	CG	N/A	0.92	21.62	76	15.03	14
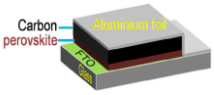	HP[c)]	N/A	N/A	1.00	21.30	63	13.53	23
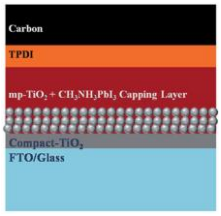	DBT[e)]	CCP[d)]	N/A	1.03	20.1	75	15.5	15
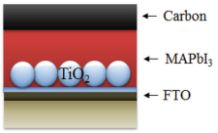	Printing	CCP	0.07 1	1.04 0.99	21.27 19.63	65 50	14.38 9.72	24
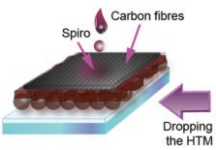	SW[b)]	CCP	0.16	1.12	20.4	67	15.3	10

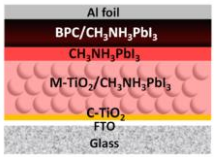	HP	Carbon carbonized at 900 °C	0.25	0.90	12.35	61	6.78	27
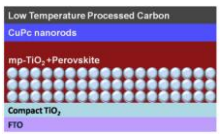	DBT	CCP	0.09	1.05	20.8	74	16.1	16
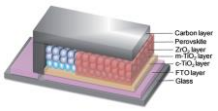	SP	CG	0.13	1.00	19.31	74	14.35	36
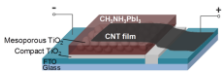	SW	CNT	0.16	1.00	18.1	55	9.90	37
4. Spiro-OMeTAD drop-casting 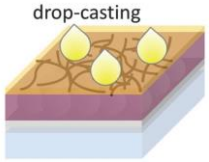	SW	CNT	0.16	1.10	20.3	61	13.6	21
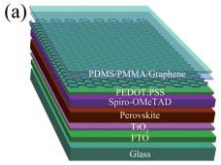	HP	CVD Graphene	0.10	0.96	19.17	67	12.37	7
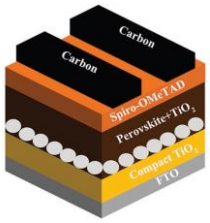	HP	CCP	0.1	1.08	23.33	76	19.2	22
Corresponding planar device			0.1	1.03	23.02	73	17.47	

[a] SP: Screen-printing; [b] SW: Solvent welding; [c] HP: Heat-Pressing; [d] CCP: Commercial Carbon Paste; [e] DBT: Doctor–Blading Technique; [f] CG: Carbon black/Graphite

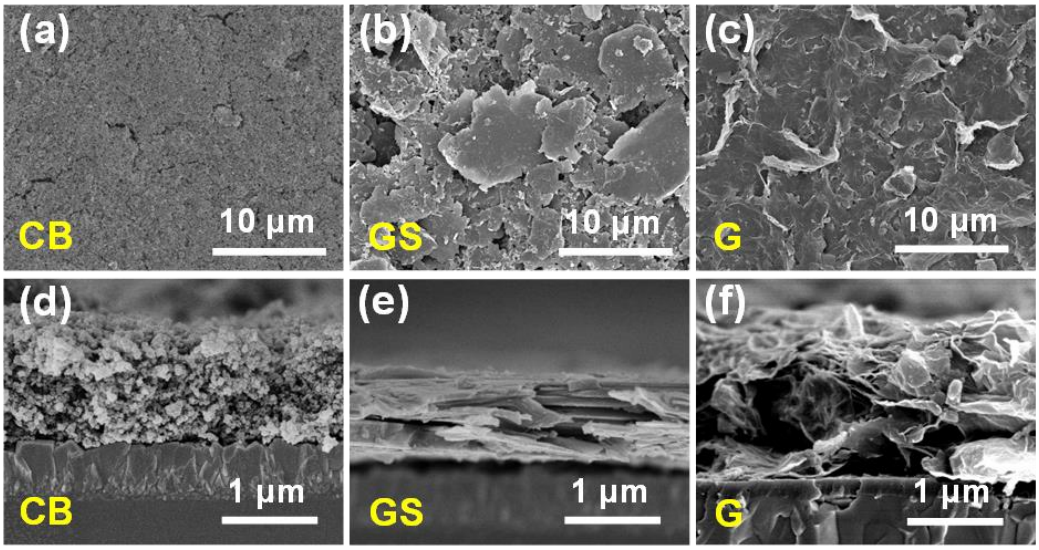

Fig. S1. The top-view (a-c) and corresponding cross-section (d-f) SEM images of carbon films obtained from diverse carbon sources (CB, GS and G).

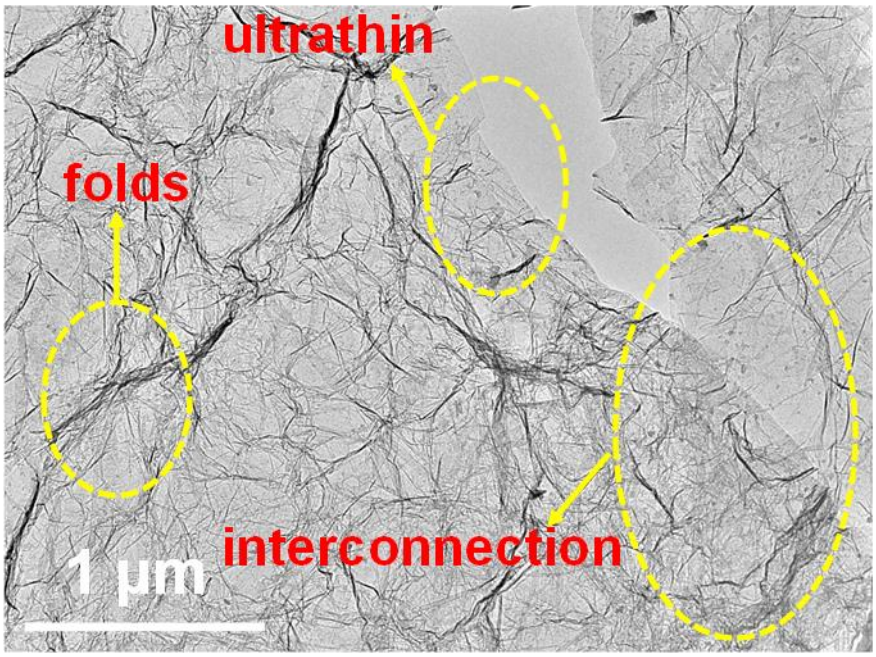

Fig. S2. TEM image of graphene.

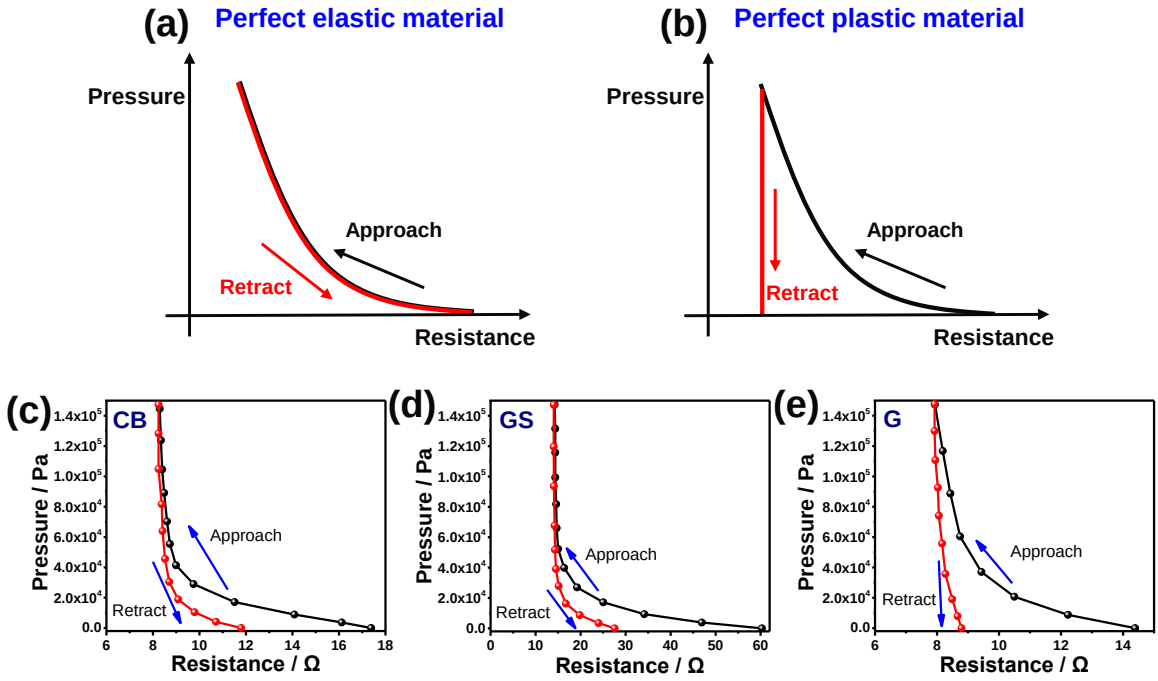

Fig. S3. The resistance-pressure curves measured during from approaching and retracting process. (a) perfect elastic material, (b) perfect plastic material, (c-e) stacked C-based symmetrical cells with various carbon sources (CB, GS and G).

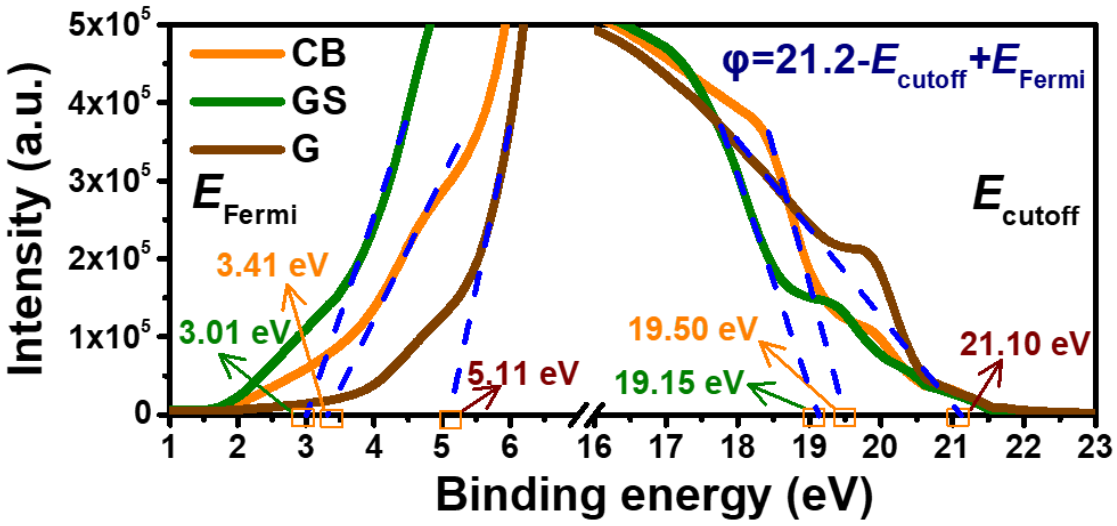

Fig. S4. UPS spectra of carbon films with various carbon sources (CB, GS and G), showing the Fermi edge (left part) and cut-off energy (right part).

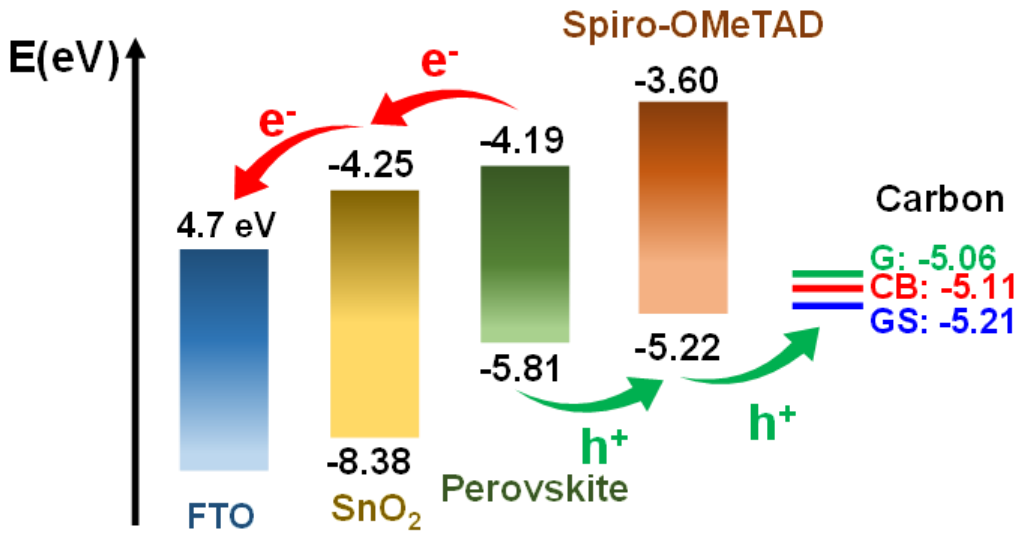

Fig. S5. Schematic band energy alignment of the C-PSCs (semi-cell A) with different carbon sources (CB, GS and G).

Table S3. Parameters of the TRPL spectra (Fig. 2c) based on perovskite, perovskite/carbon sample (CB, GS or G), perovskite/spiro-OMeTAD, respectively. The carrier lifetime was obtained by fitting TRPL spectra using a bi-exponential rate law[32]:

$$f(t)=A_1 \exp((-t)/\tau_1)+A_2 \exp((-t)/\tau_2)+B$$

$$\tau_{ave} = (A_1 \tau_1^2 + A_2 \tau_2^2)/(A_1 \tau_1 + A_2 \tau_2)$$

Samples	A_1	τ_1[ns]	A_2	τ_2[ns]	τ_{ave} [ns]
Perovskite	0.52	47.44	0.48	330.74	292.02
Perovskite/C (CB)	0.53	19.03	0.47	90.62	77.03
Perovskite/C (GS)	0.56	38.66	0.44	217.02	183.65
Perovskite/C (G)	0.60	18.02	0.40	77.72	62.14
Perovskite/spiro-OMeTAD	0.67	5.47	0.33	22.42	16.86

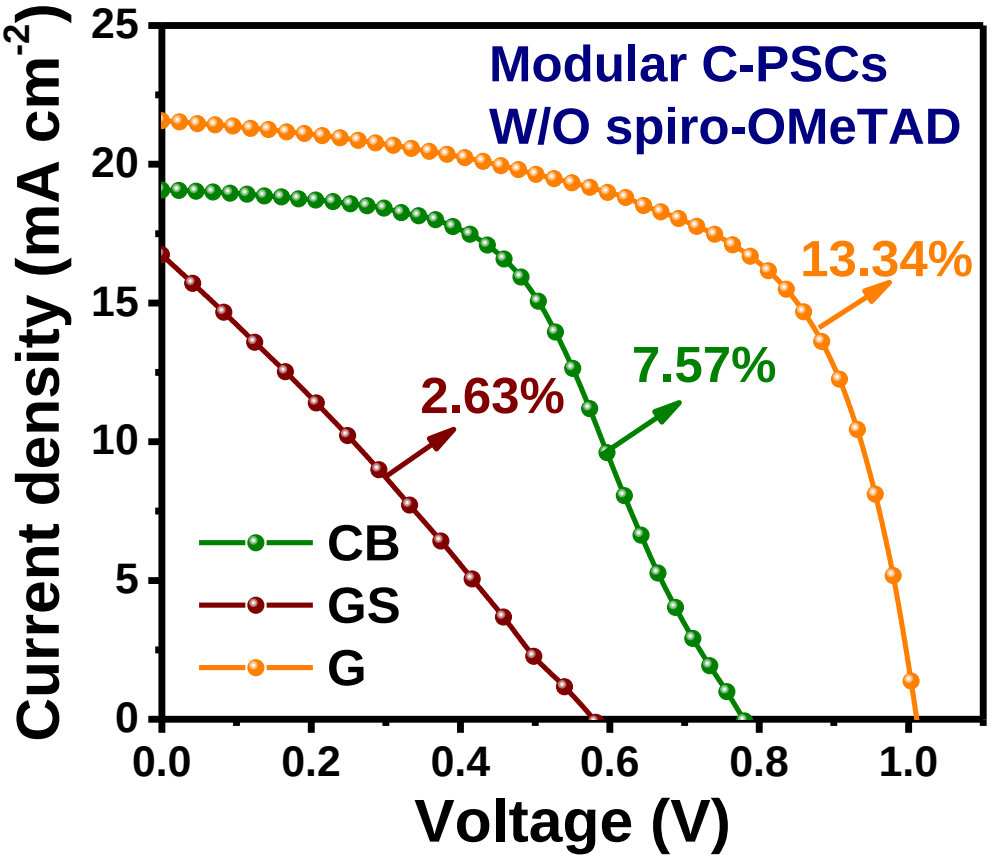

Fig. S6. *J-V* curves measured under solar simulator AM 1.5 for modular C-PSCs without spiro-OMeTAD layer based on different carbon sources (CB, GS and G).

Table S4. Detailed parameters of modular C-PSCs without spiro-OMeTAD layer based on different carbon sources (CB, GS and G).

Carbon materials	V_{oc} [V]	J_{sc} [mA cm^{-2}]	FF [%]	PCE [%]
Modular C-PSC (CB)	0.75	19.05	53	7.57
Modular C-PSC (GS)	0.54	15.71	31	2.63
Modular C-PSC (G)	1.00	21.52	62	13.34

Table S5. Parameters of the TRPL spectra (Fig. 2d) based on perovskite/spiro-OMeTAD, perovskite/spiro-OMeTAD/carbon samples with diverse carbon sources (CB, GS and G). The carrier lifetimes for the perovskite were obtained by fitting TRPL spectra using an ential eqn[32]:

$$f(t)=A_1 \exp((-t)/\tau_1)+A_2 \exp((-t)/\tau_2)+B$$

$$\tau_{ave} = (A_1 \tau_1^2 + A_2 \tau_2^2)/(A_1 \tau_1 + A_2 \tau_2)$$

Samples	A_1	τ_1[ns]	A_2	τ_2[ns]	τ_{ave} [ns]
Perovskite/spiro-OMeTAD	0.67	5.47	0.33	22.42	16.86
Perovskite/spiro-OMeTAD/C (CB)	0.65	4.98	0.35	19.26	14.56
Perovskite/spiro-OMeTAD/C (GS)	0.72	4.85	0.28	21.26	15.25
Perovskite/spiro-OMeTAD/C (G)	0.71	4.48	0.29	18.39	13.24

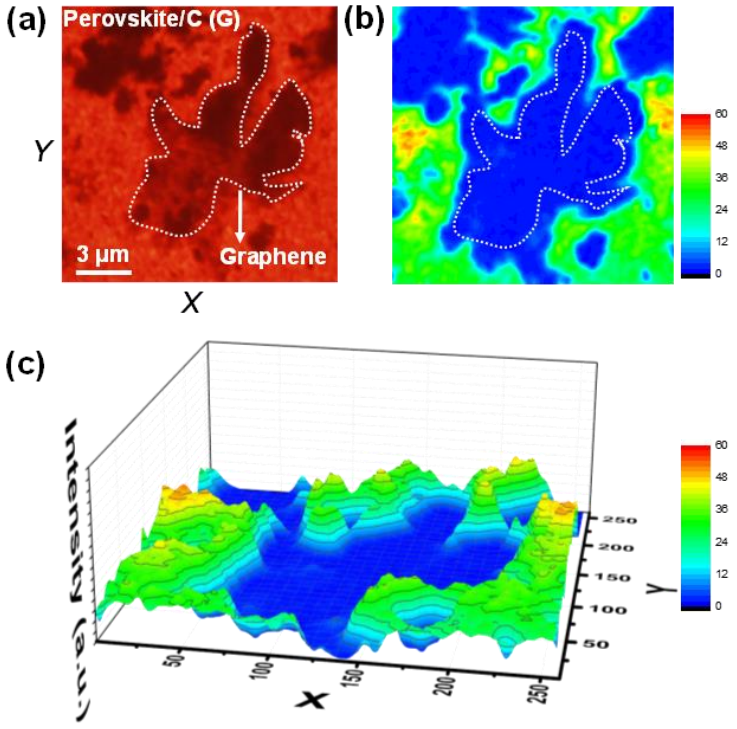

Fig. S7. Optical images (a), 2D PL mapping of intensity (b) and 3D PL mapping of intensity (c) based on the perovskite/C (graphene).

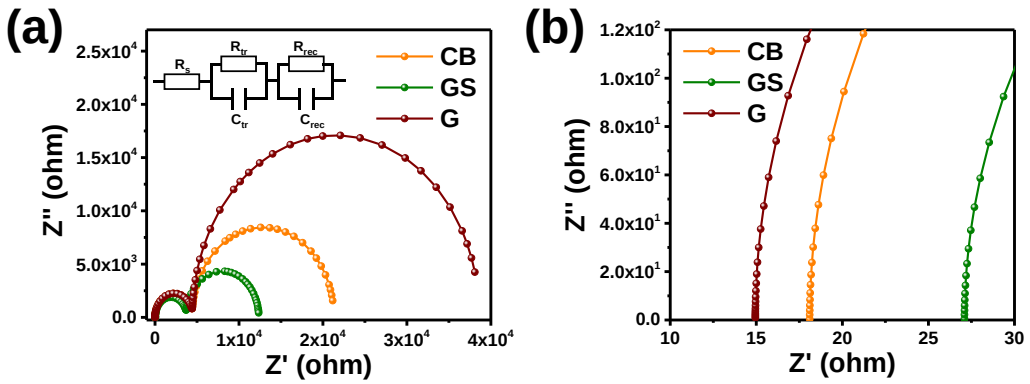

Fig. S8. (a) Nyquist plots of device based on different electrodes in dark condition at an applied bias of 300 mV and the equivalent circuit employed to fit the spectra. R_s is series resistance, R_{tr} is related to charge transport resistance and R_{rec} is related to charge recombination resistance. (b) Enlarged view of the high frequency region.

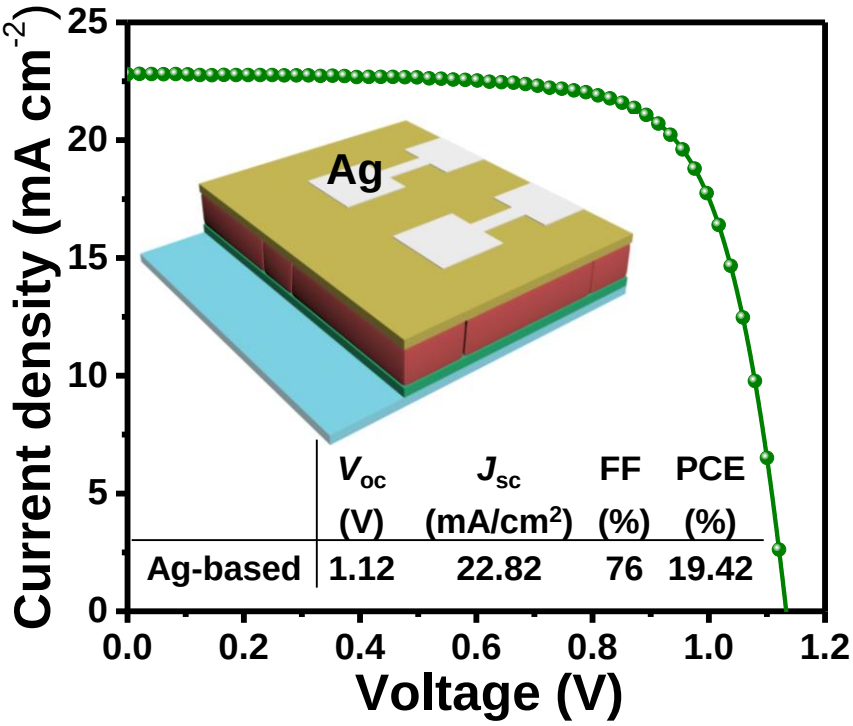

Fig. S9. *J-V* characteristics of PSCs with high-vacuum evaporated Ag as electrode.

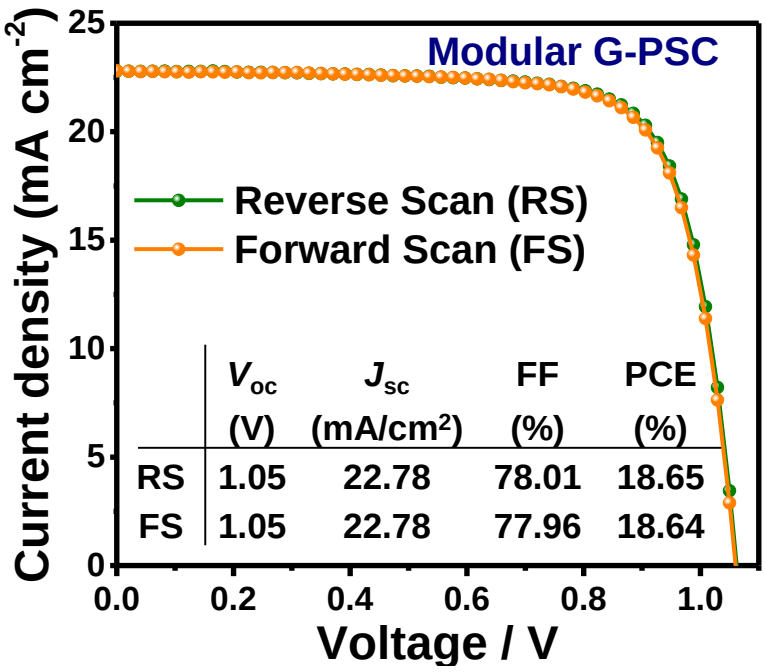

	V_{oc} (V)	J_{sc} (mA/cm^2)	FF (%)	PCE (%)
RS	1.05	22.78	78.01	18.65
FS	1.05	22.78	77.96	18.64

Fig. S10. *J-V* characteristics measured under solar simulator AM 1.5 for modular G-PSC with forward scan (FS) and reverse scan (RS). Inset shows the photovoltaic performance parameters extracted from the FS and RS curves.

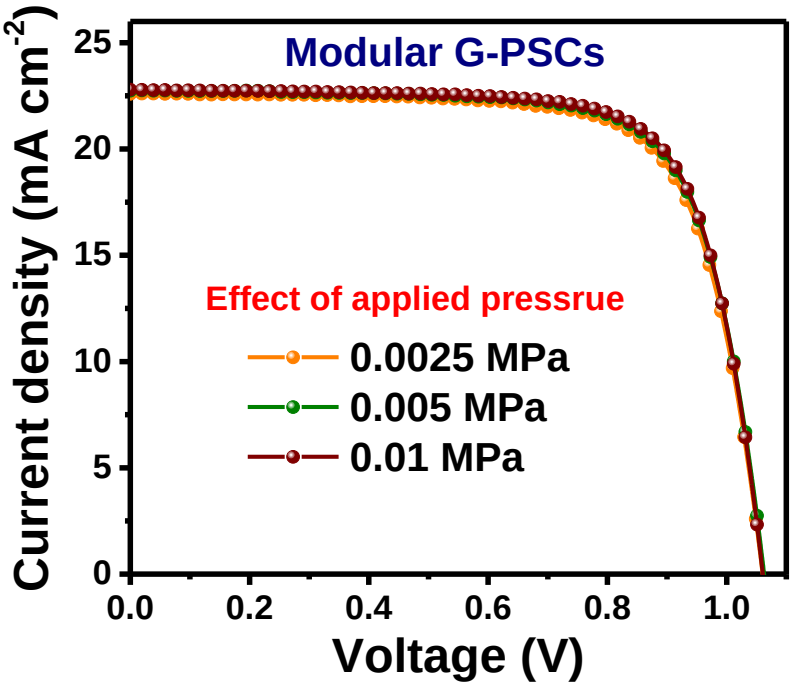

Fig. S11. *J-V* curves of the corresponding modular G-PSCs under different assembly pressures.

Table S6. Performance parameters of the corresponding modular G-PSCs under different assembly pressures.

Pressure (MPa)	V_{oc} [V]	J_{sc} [mA cm^{-2}]	*FF* [%]	*PCE* [%]
0.0025	1.05	22.61	77	18.28
0.005	1.05	22.75	78	18.63
0.01	1.05	22.78	78	18.65

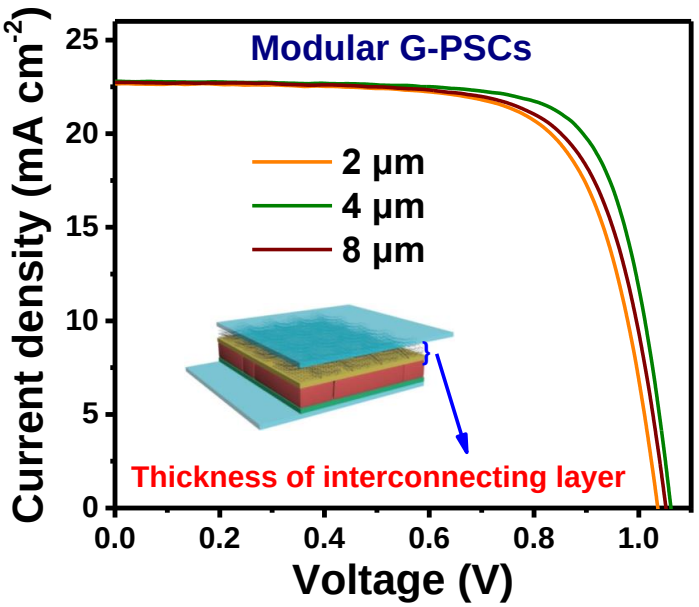

Fig. S12. Performance parameters of the modular G-PSCs with different thickness interconnecting layer.

Table S7. Performance parameters of the modular G-PSCs with different thickness interconnection layer.

Thickness (μm)	V_{oc} [V]	J_{sc} [mA cm^{-2}]	*FF* [%]	*PCE* [%]
2	1.03	22.67	74	17.27
4	1.05	22.78	78	18.65
8	1.04	22.73	75	17.72

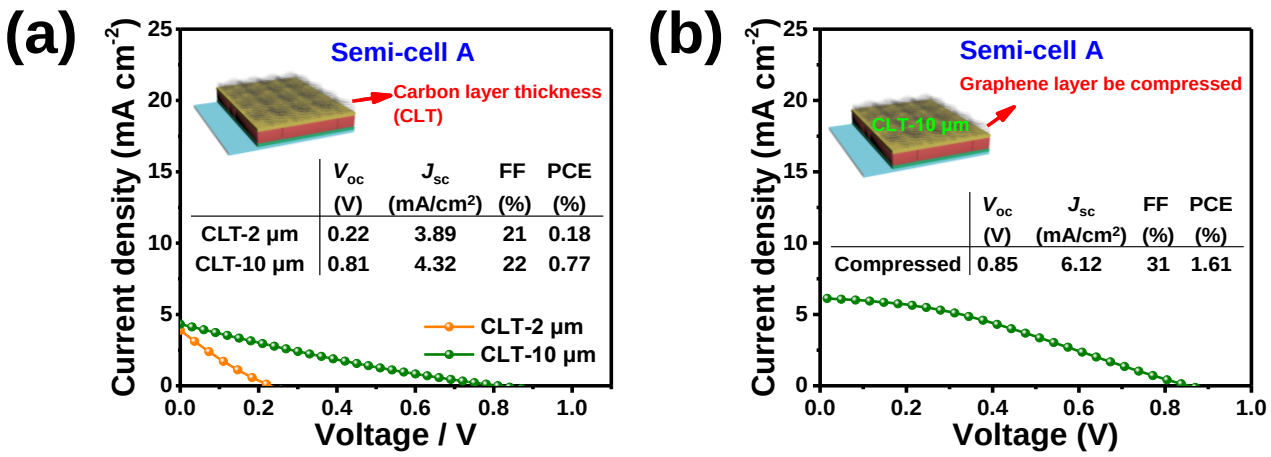

	V_{oc} (V)	J_{sc} (mA/cm²)	FF (%)	PCE (%)
CLT-2 μm	0.22	3.89	21	0.18
CLT-10 μm	0.81	4.32	22	0.77

	V_{oc} (V)	J_{sc} (mA/cm²)	FF (%)	PCE (%)
Compressed	0.85	6.12	31	1.61

Fig. S13. (a) *J-V* characteristics of semi-cell A with different carbon layer thickness (CLT), (b) *J-V* characteristics of semi-cell A after the CLT-10 μm carbon film in the semi-cell A is compressed.

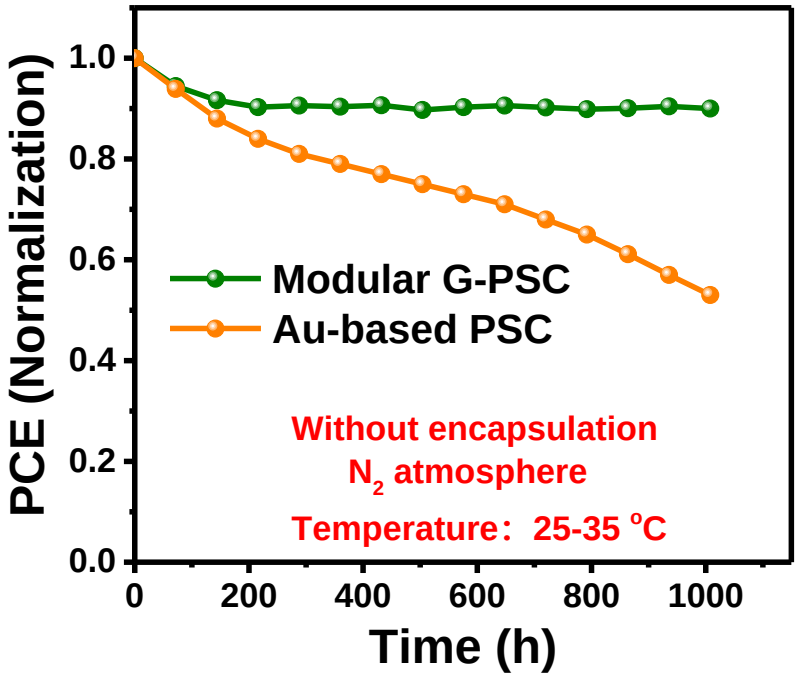

Fig. S14. Stability test of Au-based PSC and modular G-PSC under 1-sun light continuous illumination.

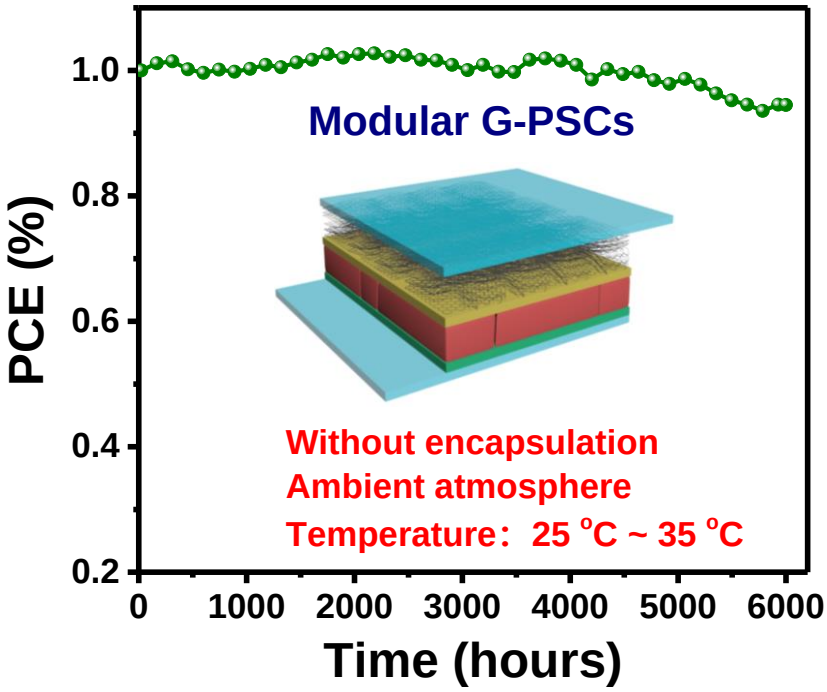

Fig. S15. Shelf life tests for modular G-PSC without encapsulation stored in the ambient air (25 °C ~ 35 °C, 40% ~ 80% humidity).

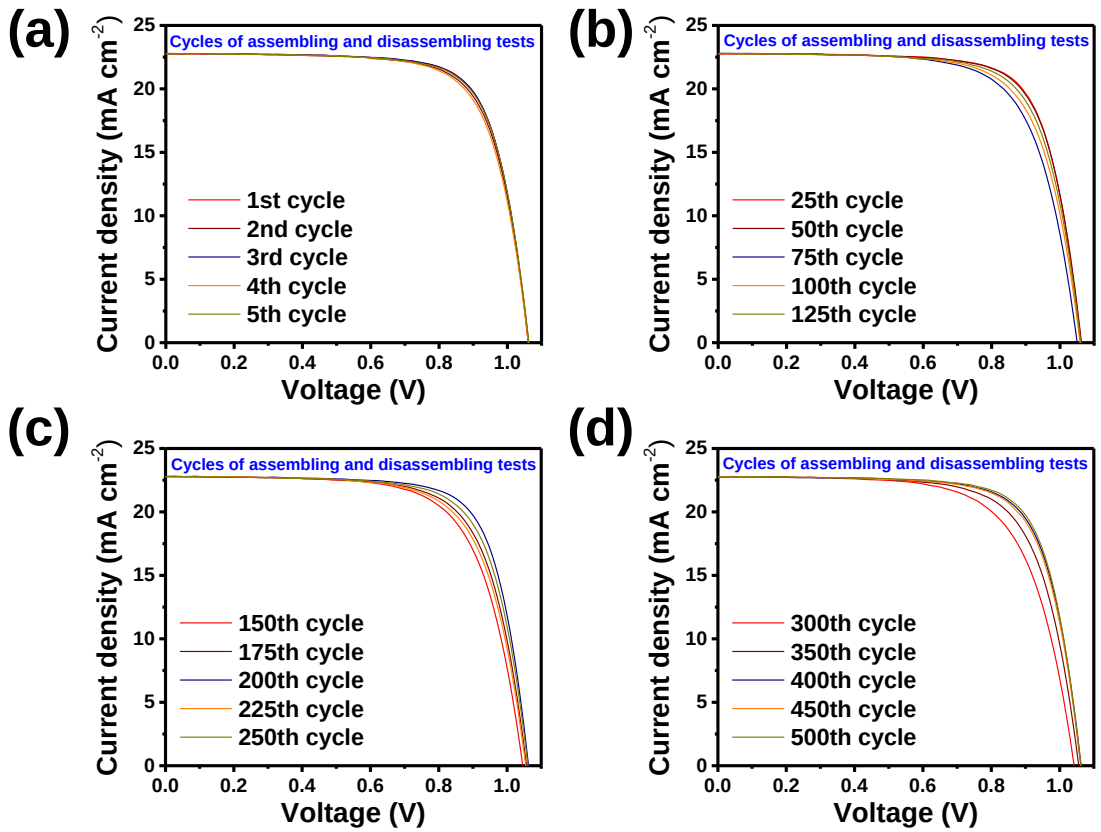

Fig. S16. Evolution of *J-V* curves of modular G-PSC after various cycles of assembling and disassembling tests.

Table S8. Evolution of performance parameters of modular G-PSC after various cycles of assembling and disassembling tests.

Cycles	V_{oc} [V]	J_{sc} [mA cm^{-2}]	*FF* [%]	*PCE* [%]
1st	1.05	22.78	77.6	18.56
2nd	1.05	22.73	76.7	18.31
3rd	1.05	22.78	77.6	18.56
4th	1.05	22.74	75.8	18.09
5th	1.05	22.76	77.2	18.45
25th	1.05	22.74	77.4	18.48
50th	1.05	22.77	76.9	18.39
75th	1.03	22.79	73.4	17.23
100th	1.05	22.76	73.8	17.64
125th	1.05	22.79	75.5	18.07
150th	1.03	22.81	72.3	16.99
175th	1.05	22.79	73.7	17.64
200th	1.05	22.78	77.5	18.54
225th	1.05	22.75	72.6	17.34
250th	1.05	22.76	75.6	18.07
300th	1.03	22.76	70.6	16.55
350th	1.05	22.76	73.4	17.55
400th	1.05	22.76	76.7	18.33
450th	1.05	22.77	76.1	18.19
500th	1.05	22.74	77.7	18.55

Table S9. Sheet resistances of G-charge collector B and pure G electrodes. Besides, G-charge collector B and pure G electrodes had the same thickness graphene and their sheet resistances are measured in the same way.

Sample	Sheet resistance (Ω/sq)
Pure G electrodes	2104.6
G-charge collector B	7.2

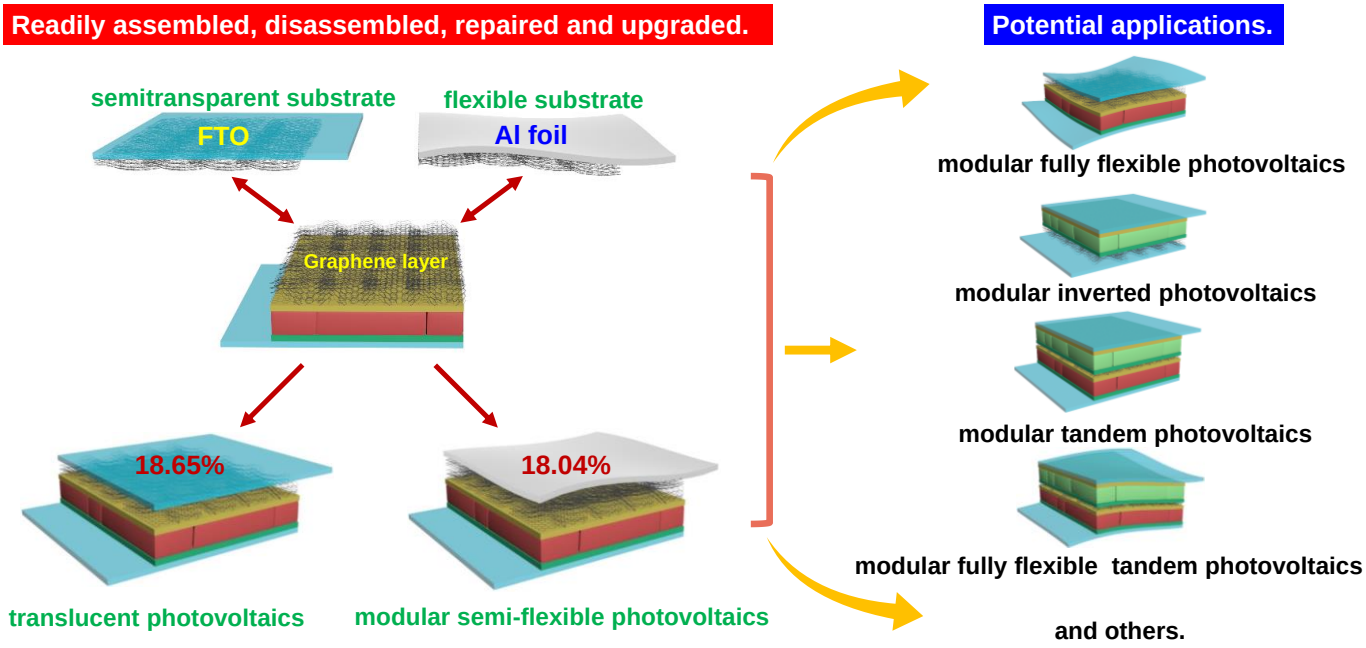

Fig. S17. Benefits and potential applications of modular architecture.